國立交通大學
電子物理學系暨研究所
碩士論文

以分子束磊晶成長之氧化錳鋅薄膜的光學特性研究

Optical Properties of ZnMnO Thin Films Grown by Molecular Beam Epitaxy

研究生 ： 楊侑霖

指導教授 ： 周武清 教授

中華民國一百零一年六月

以分子束磊晶成長之氧化錳鋅薄膜的光學特性研究

Optical Properties of ZnMnO Thin Films Grown by Molecular Beam Epitaxy

研究生 ： 楊侑霖　　Student: Yu-Lin Yang

指導教授 ： 周武清 教授　　Advisor: Prof. Wu-Ching Chou

國立交通大學

電子物理研究所

碩士論文

A Thesis
Submitted to Institute of Electrophysics
College of Science
National Chiao Tung University
In Partial Fulfillment of the Requirements
for the Degree of
Master
in
Electrophysics

June 2012
Hsinchu, Taiwan, Republic of China

中華民國一百零一年六月

以分子束磊晶成長之氧化錳鋅薄膜的光學特性研究

研究生：楊侑霖　　指導教授：周武清 教授

國立交通大學電子物理學系暨研究所

摘要

本篇論文利用分子束磊晶系統在藍寶石基板上成長氧化鋅、氧化錳鋅薄膜。由 X 光繞射的實驗結果得知薄膜均為 c 軸方向的成長而且沒有第二相的產生。穿透光譜顯示氧化錳鋅的能隙隨著摻雜錳濃度的增加而有藍位移的趨勢。在共振拉曼光譜中我們發現氧化鋅樣品和氧化錳鋅樣品各自有 5 個和 11 個縱向光學聲子的訊號。藉由變溫共振拉曼光譜的實驗，可以得知縱向光學聲子訊號的強度與氧化錳鋅的能隙位置相關。除此之外，我們也對摻雜錳濃度 0.3 %的氧化錳鋅薄膜量測在磁場下的光激螢光光譜，在 0 T 和 0.3 T 時分別有 0 %和 1.4 %的圓形極化率。

Optical Properties of ZnMnO Thin Films Grown by Molecular Beam Epitaxy

Student: Yu-Lin Yang Advisor: Prof. Wu-Ching Chou

Department of Electrophysics

National Chiao Tung University

Abstract

$Zn_{1-x}Mn_xO$ (x = 0 ~ 0.03) thin films were grown by molecular beam epitaxy (MBE) system. X-ray diffraction (XRD) result reveals that these samples are all grown along *c*-axis and there are no second phases. Transmittance shows an increase of the band gap with the increasing Mn concentration. The resonant Raman scattering (RRS) spectra showed that there are 5 and 11 longitudinal optical (LO) phonon lines for ZnO and $Zn_{1-x}Mn_xO$ samples, respectively. The LO phonon line intensity is sensitive to the band gap position as shown in the RRS spectra. Furthermore, for the $Zn_{0.997}Mn_{0.003}O$ sample, the circular polarization

degrees are P = 0 % and 1.4 % in magnetic field B = 0 T and 0.3 T, respectively.

誌謝

很快地碩士班兩年過去了，現在我即將離開這個充滿回憶的地方。回想起來，很多場景依然清晰好似才剛經歷過似的。而在這一片一片的風景中我很慶幸能和大家一起分享。

求學的過程是辛苦的，尤其在浩瀚無垠的知識大海中尋找、追逐，很多時候真會因為錯過了可能的線索而感到氣餒，但在知道自己終於摸著了一點痕跡時又會為此欣喜若狂。而在這旅途中我尤其感謝大家的陪伴和包容。

感謝周武清老師在兩年前讓我加入分子束磊晶實驗室，在這裡有豐沛的研究資源，尤其有精密且昂貴的分子束磊晶系統。在碩一時老師也讓我有這機會參加舉辦於日本仙台的學術研討會。在這研討會期間我除了上台報告、聽許多外國學者演講之外，也參觀了國外知名研究團隊的實驗室，這次的日本行真的是很特別的經驗。另外也很感激老師在學生的實驗以及論文部分的指導，藉由和老師的討論我學得作學術研究所應有的嚴謹態度。

我也感謝林彥丞學長，在我因為實驗數據而感到困惑時提供我正確的方向，以及簡崑峰學長教導我樣品的製備和分子束磊晶的操作流程。另外也感謝李寧學長、范文忠學長、辜瑞泰學長、鄒安傑學長教

導我操作實驗儀器以及提供建議。我也謝謝同是碩二生的維綸、蓉霏，以及小育、宣劭、湘穎、嘉華、明叡，藉由和你們聊天在這研究過程中才因此充滿了樂趣。

最後我要感謝我的奶奶、爸爸、媽媽、姐姐和弟弟，自小讀書至今已十八年，因為有你們的鼓勵和支持，我才能有這些成就，我心懷感激，也期待能和你們一同分享榮耀。

Contents

Chapter 1 Introduction

1.1 Background

Diluted magnetic semiconductors (DMS) have been intensely studied in the last few decades. By introducing the magnetic atoms to substitute the cations of the binary semiconductors, such as II-VI or III-V compound semiconductors, the band gaps can be varied and the semiconductors also exhibit very interesting magnetic effects [1]. Among II-VI DMS, zinc manganese oxide (ZnMnO) has direct band gap (above 3.37 eV at 300 K) and large exciton binding energy (near 60 meV) [2]. Furthermore, Mn^{2+} ion has half-filled 3*d*-orbital with five electrons in the same spin direction, therefore it has the large total spin angular momentum (S = 5/2). These advantages make ZnMnO a potential material for applications in spintronics such as spin light-emitting diodes (spin LEDs) and spin filters. Recently, there are some papers focused on the magnetic properties of ZnMnO because of the prediction of room temperature ferromagnetism [3], however optical properties of ZnMnO are still rarely studied. In this thesis, resonant Raman scattering and photoluminescence of ZnMnO with variant Mn concentration are investigated.

1.2 Paper reviews and motivations

Resonant Raman scattering (RRS) is a very special optical phenomena of semiconductors. RRS experiments of pure ZnO or ZnMnO have been studied in recent years [4-7]. From RRS spectra, there are only longitudinal optical (LO) phonon lines rather than some conventional phonon characteristics in normal Raman spectra [8]. It is mainly because of the polar symmetry of LO phonon modes in wurtzite $Zn_{1-x}Mn_xO$ ($x \geqq 0$) structure (Fig. 1.1(a)), where the A_1(LO) or E_1(LO) phonon modes consist of both oxygen atoms and zinc atoms moving parallel or perpendicular to the *c*-axis, respectively (Fig. 1.1(b)). Previous paper [7] also reported that the enhanced RRS intensity may be related to the band gap energy, near band edge emission intensity, and intrinsic defects caused by the dopant in ZnO. Accordingly, to realize the relation between the band gap and the RRS intensity, we study RRS spectra at various temperatures.

Moreover, magneto-optical experiments of ZnMnO are also an interesting subject [9-11]. Because of Mn^{2+} ion having large total spin angular momentum, ZnMnO is expected to have giant Zeeman splitting of excitonic transitions. However, there are still some controversies about

the optical properties in magnetic field. In this thesis, low temperature PL spectra of $Zn_{0.997}Mn_{0.003}O$ at magnetic field B = 0 and B = 0.3 Tesla are investigated to study its novel magneto-optical behavior.

1.3 Organization of the thesis

In this thesis, ZnO and $Zn_{1-x}Mn_xO$ (x = 0.003 ~ 0.03) thin films were grown by molecular beam epitaxy (MBE) system. X-ray diffraction (XRD) and transmittance experiments were used to study the structural and optical properties of these samples. Moreover, low temperature (10 K) and temperature dependent RRS spectra were also studied to reveal the dependence of RRS intensity on the band gap position. Furthermore, we also study low temperature PL spectra of $Zn_{0.997}Mn_{0.003}O$ at magnetic field B = 0 and B = 0.3 Tesla to measure the circular polarization degree.

There are four chapters in this thesis. We introduce the processes of sample preparations and the detailed growth parameters in Chapter 2. The experiment results are discussed in Chapter 3. And finally, Chapter 4 is the conclusion of this thesis.

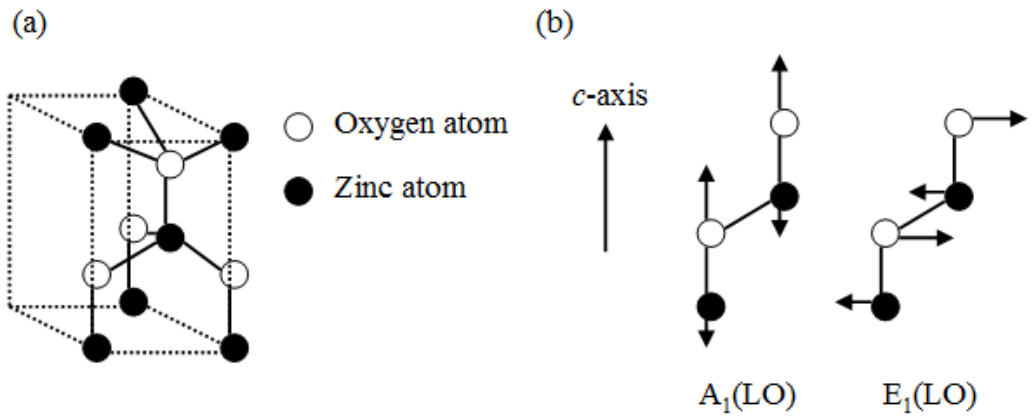

Fig. 1.1: (a) Wurtzite ZnO structure and (b) the displacement vectors of the A_1(LO) and E_1(LO) phonon modes.

Chapter 2 Experiment

2.1 Molecular beam epitaxy (MBE) system

MBE system is a growth technique in which the samples can be grown under an ultra-high vacuum condition. Within the growth process, the constituent elements of the samples will reach the substrate more directly with less collision between these elements in the chamber. Moreover, the growth rate of the samples can be very slow and the fluxes of these elements can be controlled by controlling the cell temperatures. Because of these characteristics, novel materials such as thin films, quantum wells, and quantum dots can be grown by the MBE system.

Fig. 2.1 shows the MBE system, which was made by the SVT company in the United States. The MBE system consists of an introduction chamber, a growth chamber, the vacuum systems, and some analytical devices. There are eight cells in this system. Zinc (Zn), magnesium (Mg), cadmium (Cd), tellurium (Te), selenium (Se), and manganese (Mn) are the solid cells. Oxygen (O_2) and nitrogen (N_2) are the gas cells, which are activated to plasma by RF source. The samples were grown on the heated substrate which was set to rotate for uniform growth. And there is the main shutter below the substrate, which can

prevent the deposition before the growth process.

In order to maintain ultra-high vacuum environment, the vacuum systems including several pumps were used. Two mechanical pumps were used to lower both the background pressures of the introduction and growth chambers to 1 torr. Then the turbo in the introduction chamber was used to reduce the pressure to high vacuum (< 5×10^{-8} torr), and the turbo in the growth chamber was used to lower its pressure to ultra-high vacuum (< 1×10^{-10} torr).

In this MBE system, the reflection high energy electron diffraction (RHEED) is used to monitor the deposition process on the substrate. The RHEED can also give some information about the surface morphology by showing the spotty or streaky pattern, which is projected on the phosphor screen.

2.2 Sample preparation

In this study, ZnO and $Zn_{1-x}Mn_xO$ thin films were grown on *c*-plane sapphire substrates by using plasma assisted MBE system. Before the growth, the substrates were all etched chemically in acetone and hot H_2SO_4 : H_2PO_4 = 3:1 solutions for 5 minutes and 15 minutes, respectively,

and cleaned in deionized water. Then the substrates were mounted on a molybdenum disk by using indium (In). Finally, the substrates were loaded in the introduction chamber and transferred into the growth chamber by using the transfer arm.

Fig. 2.2 shows the structure of ZnO and $Zn_{1-x}Mn_xO$ thin films. At first, the substrate was heated to 850 ℃ for desorption. Until the RHEED pattern became streaky, the substrate temperature was decreased to 650 ℃ for the growth temperature. Since the lattice mismatches of MgO between Al_2O_3 and ZnO, 9.1 % and -8.4 % respectively, are lower than that between Al_2O_3 and ZnO (18 %) [12], MgO was chosen as the buffer layer for the deposition ZnO or ZnMnO thin films.

Proper growth conditions for growing good quality ZnO are needed, before the growth of ZnMnO samples. The oxygen flow rate was 0.6 SCCM with plasma power 250 W. The Zn cell temperatures were varied to (270, 275, 280, 285, and 290 ℃) for the growth of ZnO thin films. The detailed growth conditions of ZnO thin films are listed in Table 2.1. Then we fixed the parameters of oxygen and Zn cell and changed Mn cell temperatures to grow ZnMnO thin films with variant Mn concentrations. The detailed growth conditions of ZnMnO thin films are listed in Table

2.2.

2.3 Resonant Raman scattering (RRS), photoluminescence (PL) and transmittance

Fig. 2.3 shows the experimental setup for the RRS and PL measurements. Samples were loaded in the chamber with the closed-cycle refrigerator, in which the temperature can be set in the temperature range of 10 and 300 K. The He-Cd laser with wavelength 325 nm was used as the excitation light source, and the laser beam was directed and focused by a lens (Lens1) on the samples. The PL from the samples was collected by two lenses (Lens2, Lens3) and directed to the Horiba Jobin-Yvon iHR550 0.55 m single-grating spectrometer and detected by the LN_2-cooled charge coupled device (CCD).

Fig. 2.4 shows the experimental setup for the transmittance measurement. The Xe lamp was used as the excitation light source.

2.4 Magneto-photoluminescence

Fig. 2.5 shows the experimental setup for the magneto-PL measurement. The setup was similar to that for PL measurements. The

samples were placed on a copper holder and magnets were installed on it. To analyze spin up ($\sigma+$) and spin down ($\sigma-$) polarization components of the PL from the samples, quarter wave plate and linear polarizer were used in the experiment.

Table 2.1 Growth conditions of ZnO thin films.

	T (substrate) (℃)	T (Zn) (℃)	O_2 plasma (SCCM/W)	Thickness (nm)
Sample 1-A	650	270	0.6/250	131
Sample 1-B	650	275	0.6/250	144
Sample 1-C	650	280	0.6/250	159
Sample 1-D	650	285	0.6/250	181
Sample 1-E	650	290	0.6/250	225

Table 2.2 Growth conditions of ZnMnO thin films.

	T (substrate) (℃)	T (Zn) (℃)	O_2 plasma (SCCM/W)	T (Mn) (℃)	$Zn_{1-x}Mn_xO$ (x)
Sample 2-A	650	280	0.6/250	680	0.003
Sample 2-B	650	280	0.6/250	700	0.009
Sample 2-C	650	280	0.6/250	720	0.011
Sample 2-D	650	280	0.6/250	730	0.021
Sample 2-E	650	280	0.6/250	735	0.026
Sample 2-F	650	280	0.6/250	740	0.030
Sample 2-G	650	280	0.6/250	760	0.039
Sample 2-H	650	280	0.6/250	770	0.061

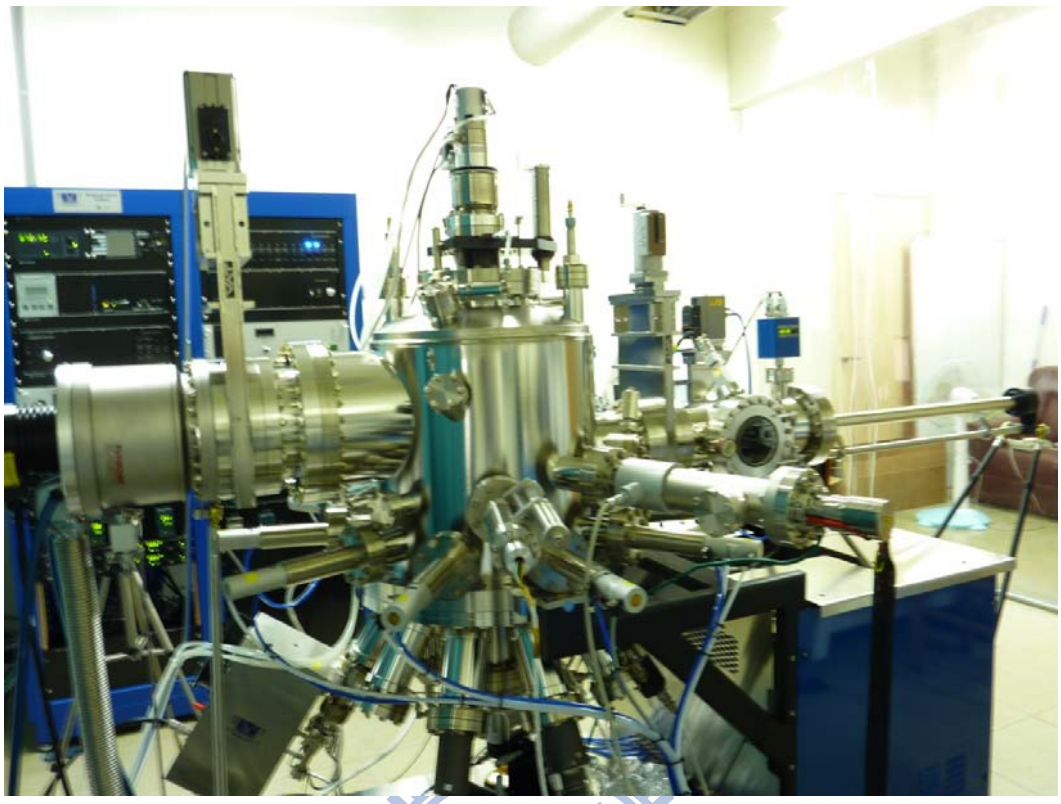

Fig. 2.1: Molecular beam epitaxy (MBE) system.

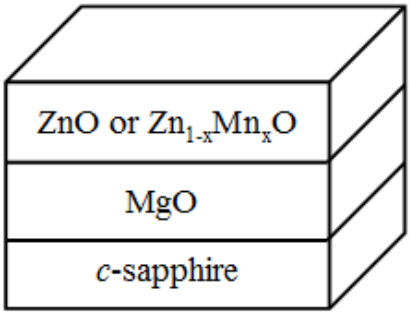

Fig. 2.2: Sample structure of ZnO or $Zn_{1-x}Mn_xO$ thin films.

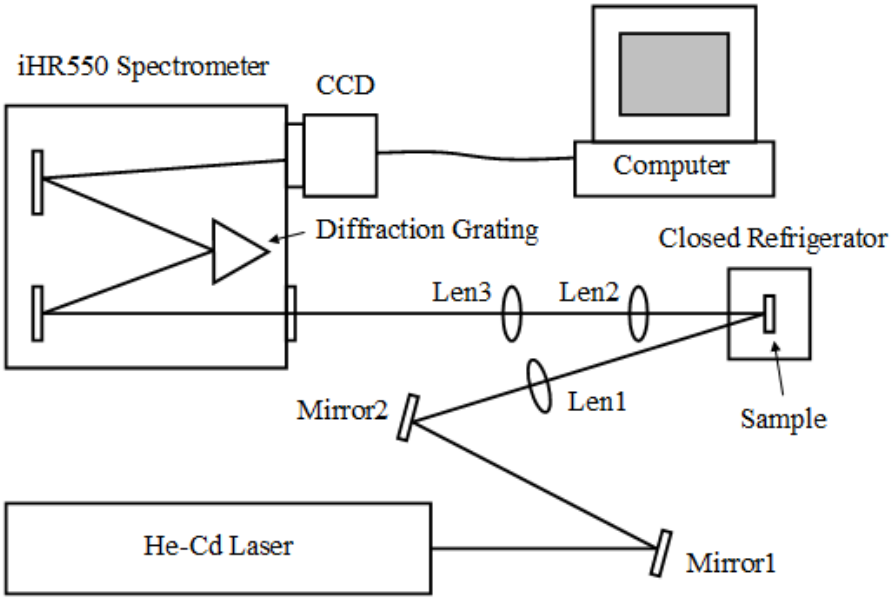

Fig. 2.3: Experimental setup for the RRS and PL measurements.

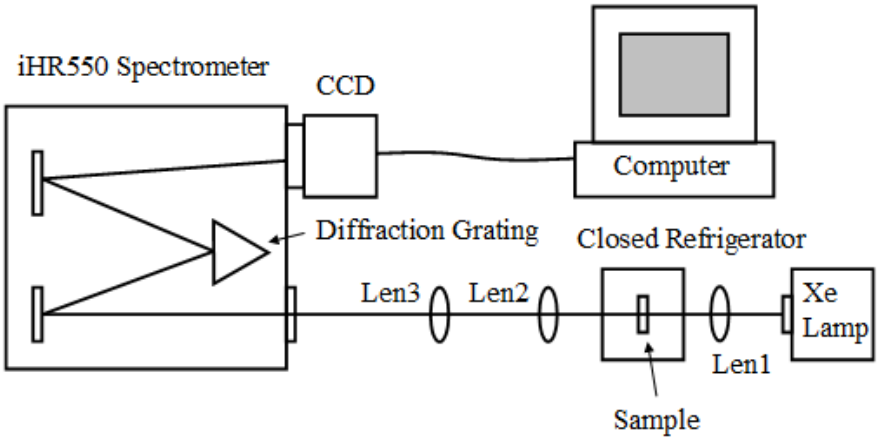

Fig. 2.4: Experimental setup for the transmittance measurement.

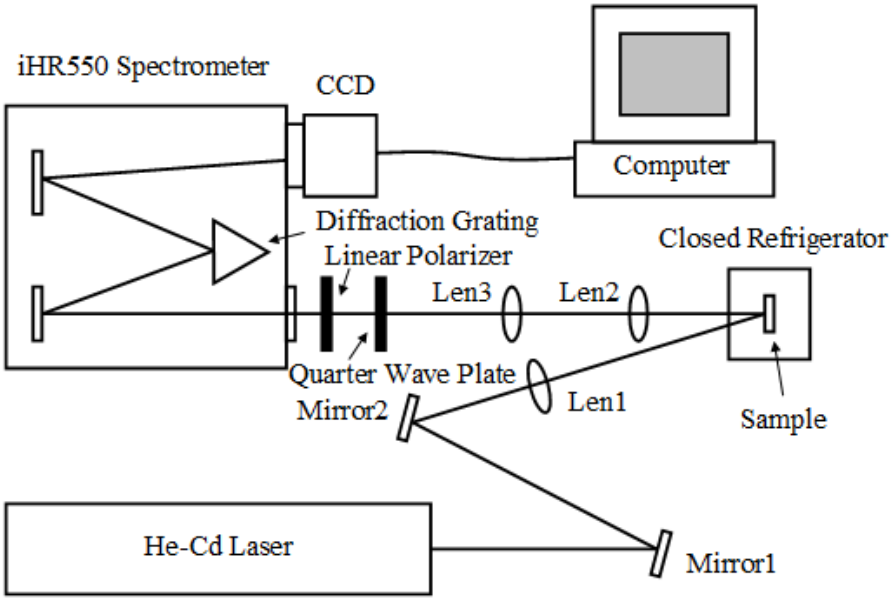

Fig. 2.5: Experimental setup for the magneto-PL measurement.

Chapter 3 Result and discussion

3.1 Growth conditions of ZnO thin films

Fig. 3.1 shows the growth rates of ZnO thin films with various Zn cell temperatures. When the substrate temperature was fixed at 650 ℃ and the oxygen flow rate was 0.6 SCCM with plasma power 250 W, the growth rate increases linearly with the increasing Zn cell temperature, which indicates these ZnO thin films were grown under oxygen-rich conditions.

The PL spectra of ZnO thin films with various Zn cell temperatures at 10 K are shown in Fig. 3.2. For these samples, the dominant peaks around 3.36 eV are attributed to the near band edge emissions (NBE) [13]. The broad and weak emissions which originate from the deep levels (DLs) near 2.25 eV are also observed. The DLs are attributed to the zinc interstitial (Zn_i), oxygen vacancy (V_O) [2], and oxygen interstitial (O_i) [14]. Fig. 3.3 shows the intensity ratios of the NBE emission to the DL emission. The intensity ratio reaches maximum value of 75 at Zn cell temperature of 280 ℃. This growth condition was used for the growth of ZnMnO epilayers.

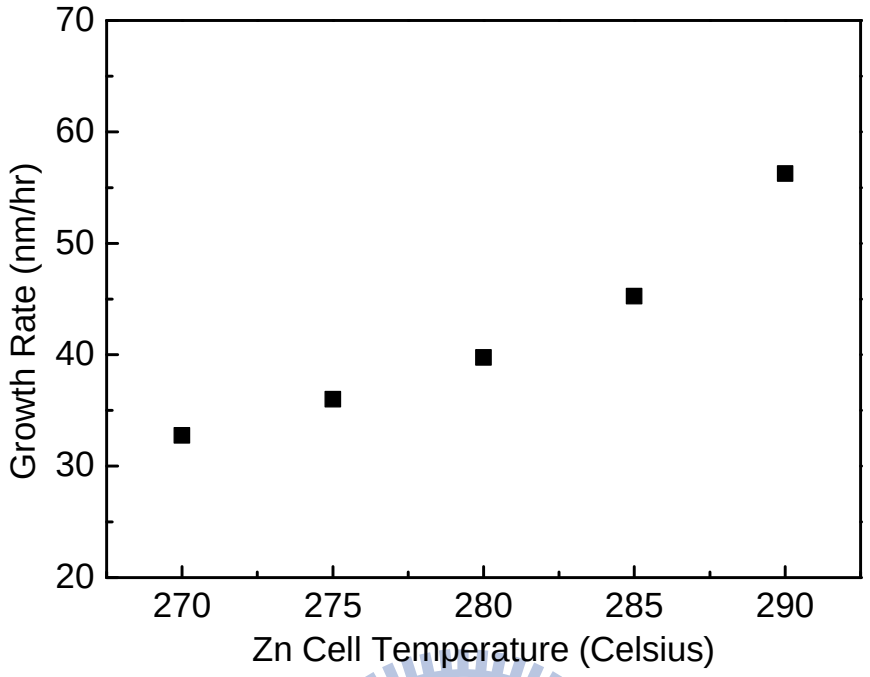

Fig. 3.1: Growth rates of ZnO thin films as a function of Zn cell temperatures.

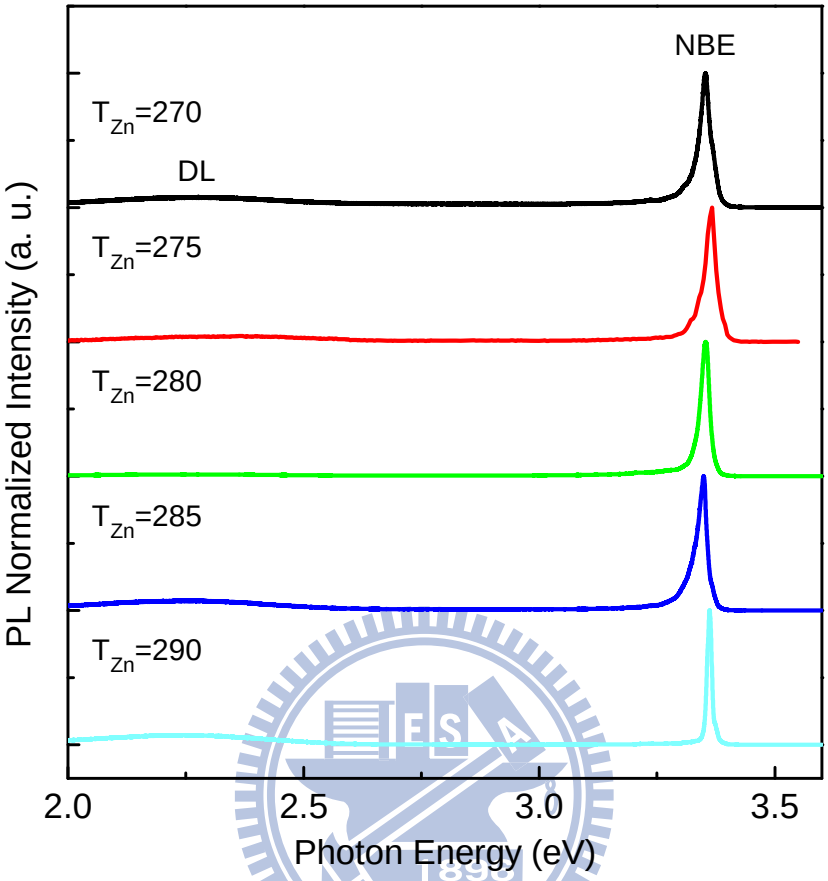

Fig. 3.2: Low temperature (10 K) PL spectra of ZnO thin films with various Zn cell temperatures.

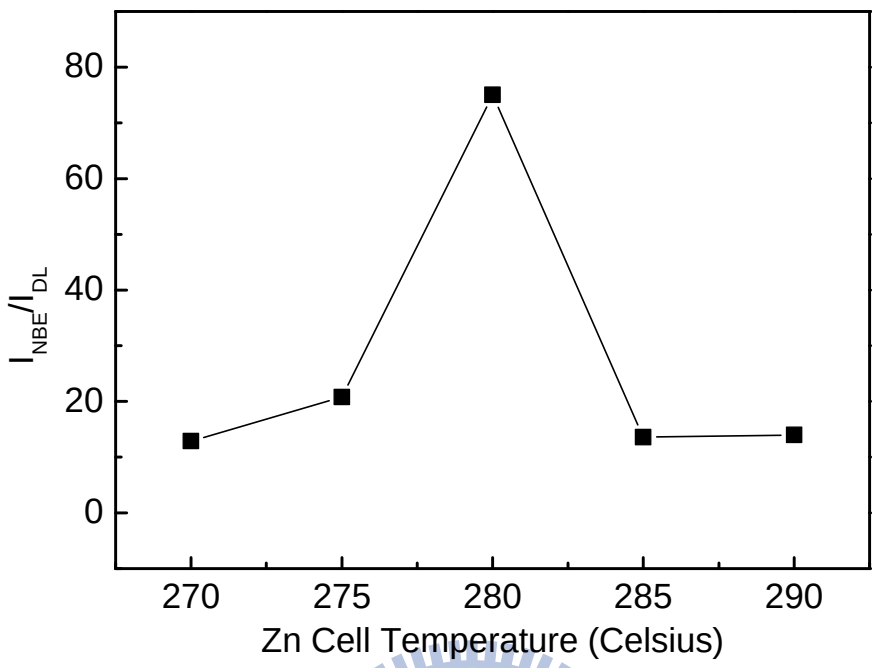

Fig. 3.3: The intensity ratios of the near band edge (NBE) emission to the deep level (DL) emission for ZnO thin films as a function of Zn cell temperatures.

3.2 Structural and optical measurements of ZnMnO thin films

3.2.1 X-ray diffraction (XRD)

Fig. 3.4 shows the XRD profile of the $Zn_{0.97}Mn_{0.03}O$ thin film. Besides the Al_2O_3 (0006) peak at 41.66°, the ZnMnO (0002) and (0004) peaks are also clearly observed at 34.21° and 72.09°, respectively. It indicates that the $Zn_{0.97}Mn_{0.03}O$ thin film was grown along the *c*-axis. There are no other peaks observed in the XRD profile, it implies that there does not exist any other crystal phase in the $Zn_{0.97}Mn_{0.03}O$ thin film.

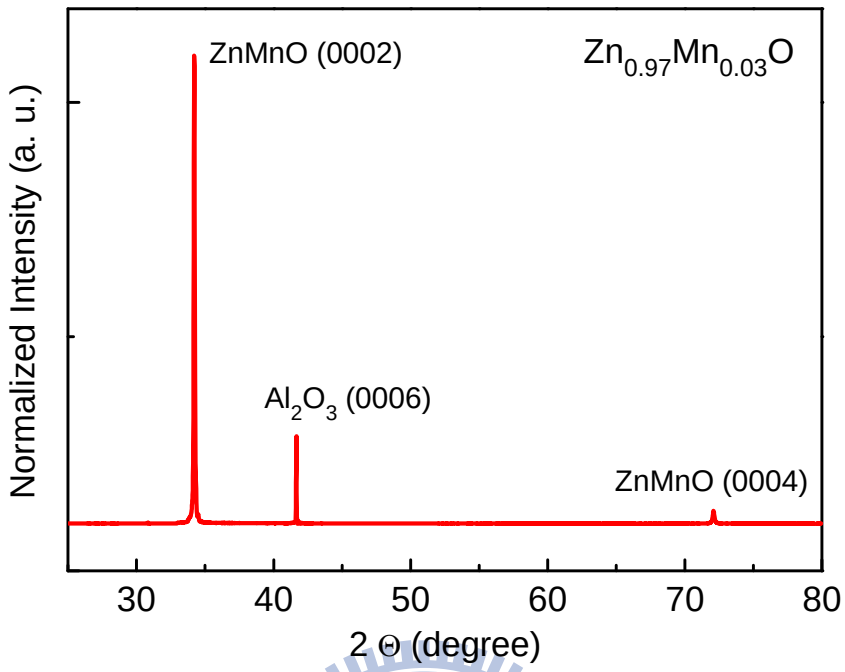

Fig. 3.4: XRD profile of the $Zn_{0.97}Mn_{0.03}O$ thin film.

3.2.2 Interband transitions

Fig. 3.5 shows room temperature transmittance spectra of $Zn_{1-x}Mn_xO$ thin films with Mn concentration x = 0, 0.009, 0.030 and 0.061. From the figure, the absorption edge energy increasing with Mn concentration can be observed. Fig. 3.6 shows the absorption edge energy of the $Zn_{1-x}Mn_xO$ versus Mn concentration. The blue shift of the absorption energy is due to MnO having a larger band gap (4.2 eV at 300 K) than ZnO (3.3 eV at 300 K) [15]. The shift of the absorption edge can be expressed by the following equation

$$E(x) = 3.337 + 3.056x\ (eV) \qquad (1)$$

The experimental results are in good agreement with reference [16]. Furthermore, the broadening of the absorption edge increases with the Mn concentration. The broadening is mainly due to the increasing disorder with increasing Mn concentration in ZnMnO. Fig. 3.5 also shows the obvious mid-gap absorption around 3 eV for higher Mn concentration samples. This effect has been ascribed to the *d-d* transitions of the Mn^{2+} ion [17].

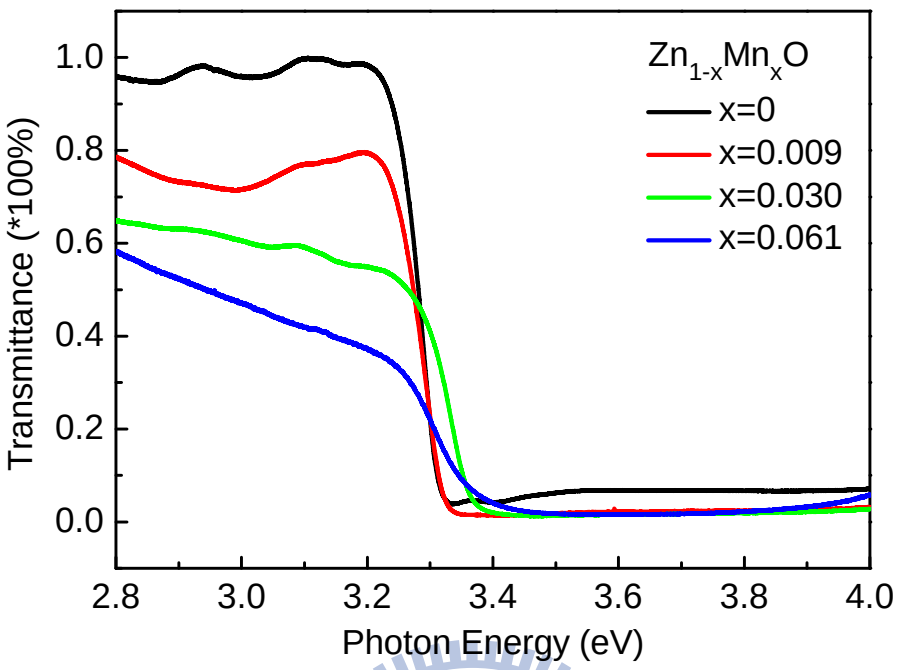

Fig. 3.5: Room temperature transmittance spectra of $Zn_{1-x}Mn_xO$ thin films with Mn concentration x = 0, 0.009, 0.030 and 0.061.

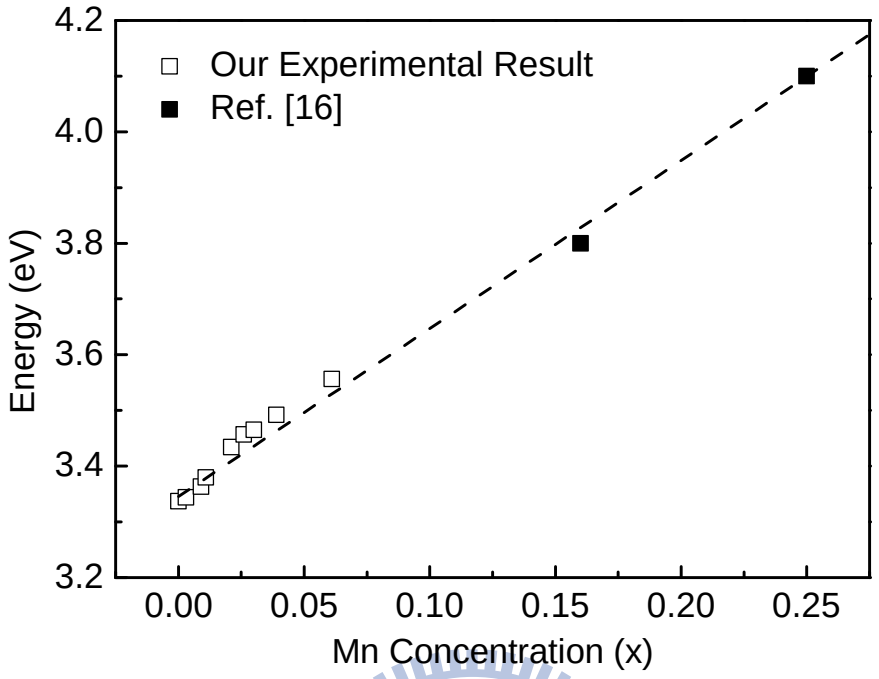

Fig. 3.6: The absorption edge energy of $Zn_{1-x}Mn_xO$ thin films as a function of the Mn concentrations (x). The experimental results of ours (□) and reference [16] (■) are plotted.

3.2.3 Multiphonon resonant Raman scattering

Fig. 3.7 shows low temperature (10 K) resonant Raman scattering (RRS) spectra of ZnO and $Zn_{0.97}Mn_{0.03}O$ thin films with the He-Cd laser (λ = 325 nm) excitation. RRS experiment is performed under the excitation laser energy higher than the band gap, and the incident photon energy will be in resonance with the electronic interband transition. The peak at 578 cm^{-1} is the first-order longitudinal optical (LO) phonon mode [8], in which both O and Zn atoms vibrate in the same direction. The weak peak around 457 cm^{-1} is ascribed to the E_2(high) mode. Compared with 440 cm^{-1} in bulk ZnO single crystal [8], the frequency of the E_2(high) mode in our sample is slightly larger, it is mainly due to strain effect in the thin film.

Under RRS condition, some intense peaks at frequency positions of approximately integer times 578 cm^{-1}, which is the frequency of the first-order LO phonon mode, contribute to the *n*th-order LO phonon scattering processes. These are intense LO phonon lines because of the Frohlich interaction, which is the interaction between electrons and the longitudinal electrical field induced by the LO phonons [18]. In addition, there are also some relatively weak peaks at frequency positions next to

these LO phonon modes. Interestingly, the intervals of these weak peaks are also close to the frequency of LO phonon mode. Considering the frequency positions of these peaks, they are probably caused by the combination of E_2(high) mode and multiple LO phonon scattering.

From the RRS spectra, we find 5 and 11 LO phonon modes for ZnO and $Zn_{0.97}Mn_{0.03}O$ samples, respectively. In previous studies [4,19], J. F. Scott *et al* believed that the LO phonon numbers (n) observed in RRS spectra varies proportionally with the electron-phonon coupling coefficient (α), which is given as the ratio of the Frohlich interaction energy to the LO phonon energy [18], and they also predicted the number of LO phonon modes in ZnO is more than $n = 9$ in CdS (see Fig. 3.8). However, they only found $n = 8$ in their ZnO sample [4]. From our results, the diversity of the LO phonon numbers in ZnO and $Zn_{0.97}Mn_{0.03}O$ may be due to the large near band edge emission intensity of ZnO sample. We can not find more LO phonon lines for $n > 5$ in ZnO. High electron-phonon coupling coefficient ($\alpha = 0.9$) of ZnO indicates electrons have large interaction energy with LO phonons, therefore the observation of large amount of LO phonon lines ($n = 11$) in RRS spectra can be understood.

Fig. 3.9 shows the RRS spectra of $Zn_{1-x}Mn_xO$ (x = 0.003 ~ 0.030) thin films. Besides some intense LO phonon lines we have mentioned before, there is an extra peak at 3632 cm^{-1} for $Zn_{0.997}Mn_{0.003}O$ sample. This peak is ascribed to the neutral donor bound exciton (D^0X). As shown in the spectra, the LO phonon mode intensity at the frequency position of around 3500 cm^{-1}, which is assigned to the sixth-order LO phonon mode, is always the largest in each of $Zn_{1-x}Mn_xO$ samples, and the intensity decreases with increasing Mn concentration. The behavior of intensity variation is mainly related to the band gap position, and it can be explained by using the Raman cross section for the *n*th-order LO phonon mode which is given as [5,20]

$$\sigma_n(\omega) = \mu^4 \sum_{j=0}^{\infty} \left| \sum_{m=0}^{\infty} \frac{\langle g, n+j | e, m \rangle \langle e, m | g, j \rangle}{E_{ex} + (m-j)\hbar\omega_{LO} - \hbar\omega_i + i\hbar\Gamma} \right|^2 \exp\left(-\frac{j\hbar\omega_{LO}}{k_B T}\right),$$

(2)

where μ is the electronic transition dipole moment, E_{ex} is the electronic transition energy, $\hbar\omega_i$ and $\hbar\omega_{LO}$ are the energies of the incident photon and the LO phonon, respectively, Γ is the homogeneous line width, $|g, n+j\rangle$ and $|g, j\rangle$ are the (*n*+*j*)th-order and *j*th-order LO phonon states in the electronic ground state, respectively, $|e, m\rangle$ is the *m*th-order LO phonon state in the electronic excited state, k_B is

Boltzmann's constant, and T is the temperature. From this equation, the nth-order LO phonon mode intensity will become larger if $E_g \cong \hbar\omega_i - n\hbar\omega_{LO}$. The band gap of $Zn_{1-x}Mn_xO$ shifts to higher energy when Mn concentration increases, and it tends to be away from the frequency position of around 3500 cm^{-1}. Therefore, the intensity of sixth-order LO phonon mode decreases.

To investigate the dependence of RRS intensity on the band gap energy, temperature dependent RRS spectra of $Zn_{0.991}Mn_{0.009}O$ is shown in Fig. 3.10(a). At 10 K, the intensity of sixth-order LO phonon mode around 3500 cm^{-1} is the largest. However, when the temperature increases to 160 K, the seventh-order LO phonon mode around 4100 cm^{-1} becomes the largest in intensity. The behavior can be explained by considering the temperature dependence of the photoluminescence (PL). Fig. 3.10(b) shows the PL peak position of $Zn_{0.991}Mn_{0.009}O$ as a function of the temperature, and the curve can be fitted by considering the Bose-Einstein statistical factor for phonons [21]

$$E(T) = E(0) - \frac{2a_B}{\exp(\Theta/T) - 1}, \qquad (3)$$

where $E(T)$ and $E(0)$ are the energies at T K and 0 K, respectively, a_B is the strength of the electron-phonon interaction, and Θ is

associated with the mean frequency of the phonons. From Fig. 3.10(a) and (b), the shift of PL position results in the LO phonon line intensity variation.

To summarize, multiple LO phonon scattering in RRS spectra can be explained by using the "cascade model" [22,23], the scattered photons will have energy $\hbar\omega \cong \hbar\omega_i - n\hbar\omega_{LO}$ or $\hbar\omega \cong \hbar\omega_i - \hbar\omega_{E_2(high)} - n\hbar\omega_{LO}$. Moreover, by studying RRS spectra, we find that when the scattered photon energy is close to the band gap, the LO phonon intensity will be resonantly enhanced.

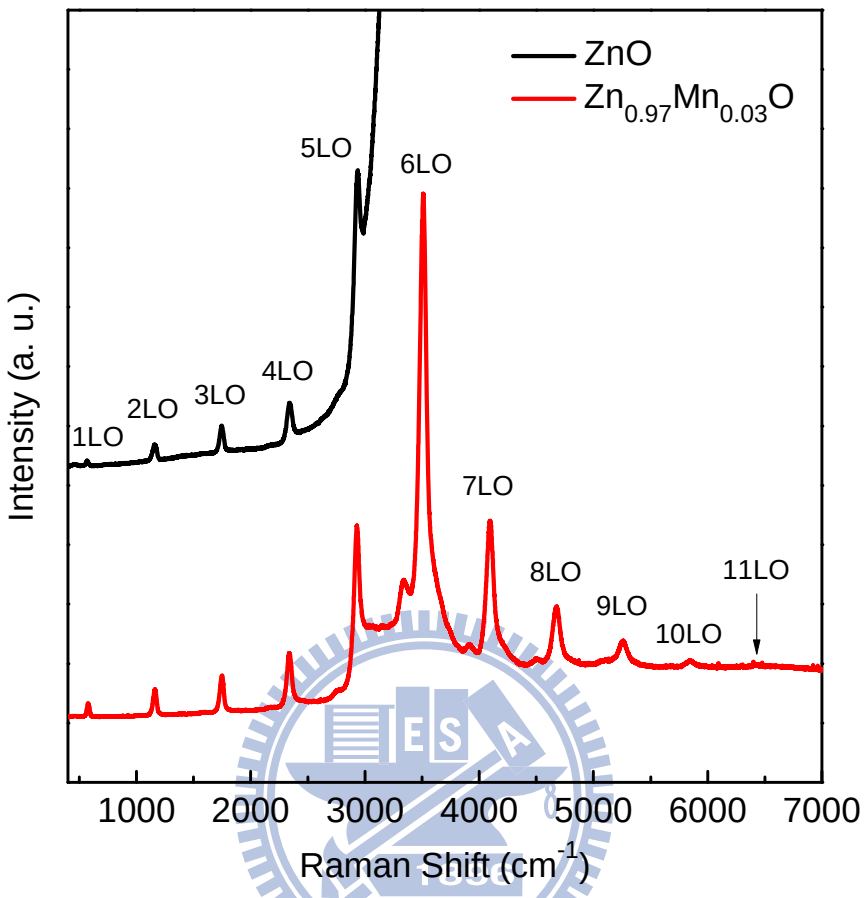

Fig. 3.7: Resonant Raman scatterings (RRS) of ZnO and $Zn_{0.97}Mn_{0.03}O$ thin films, using the He-Cd laser (λ = 325 nm).

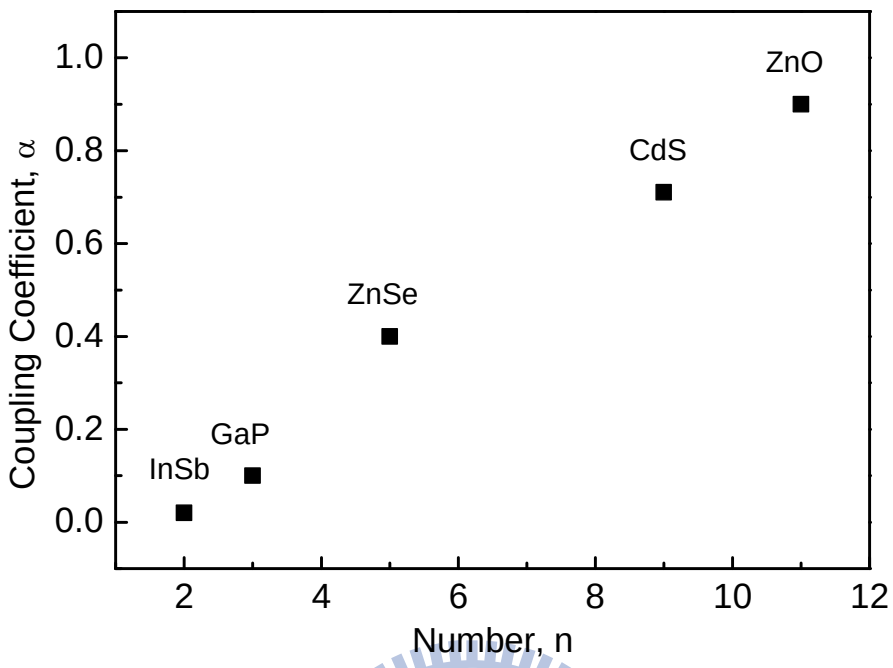

Fig. 3.8: Relation between the number of LO phonon lines (n) and the electron-phonon coupling coefficient (α) [4,19].

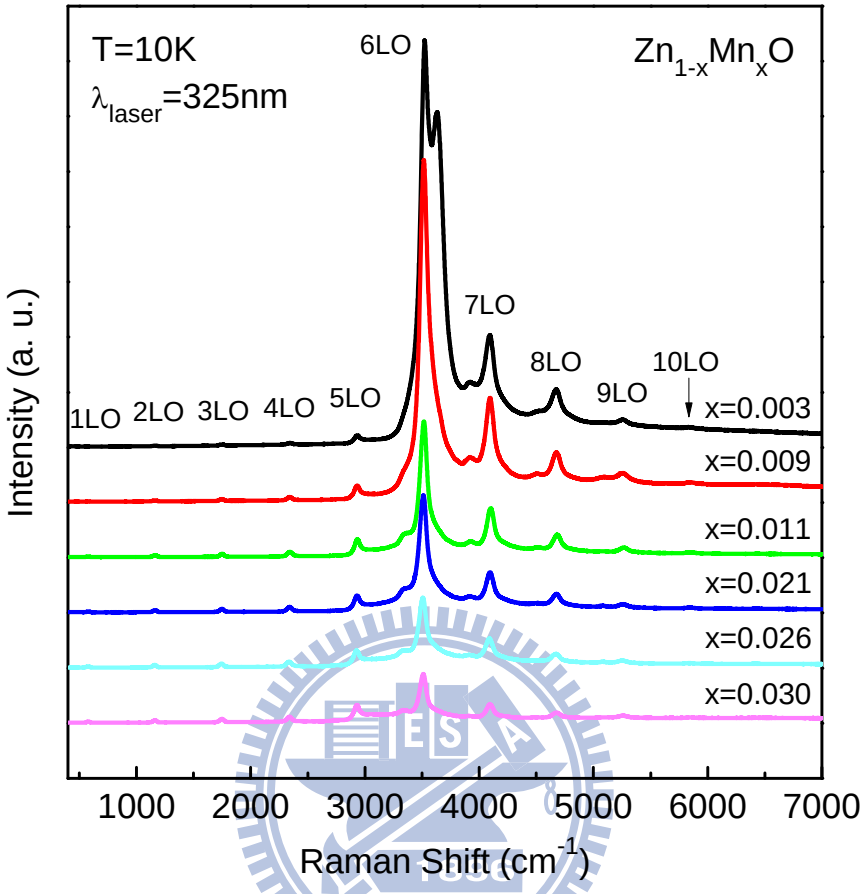

Fig. 3.9: Resonant Raman scatterings (RRS) of $Zn_{1-x}Mn_xO$ thin films, using the He-Cd laser (λ = 325 nm).

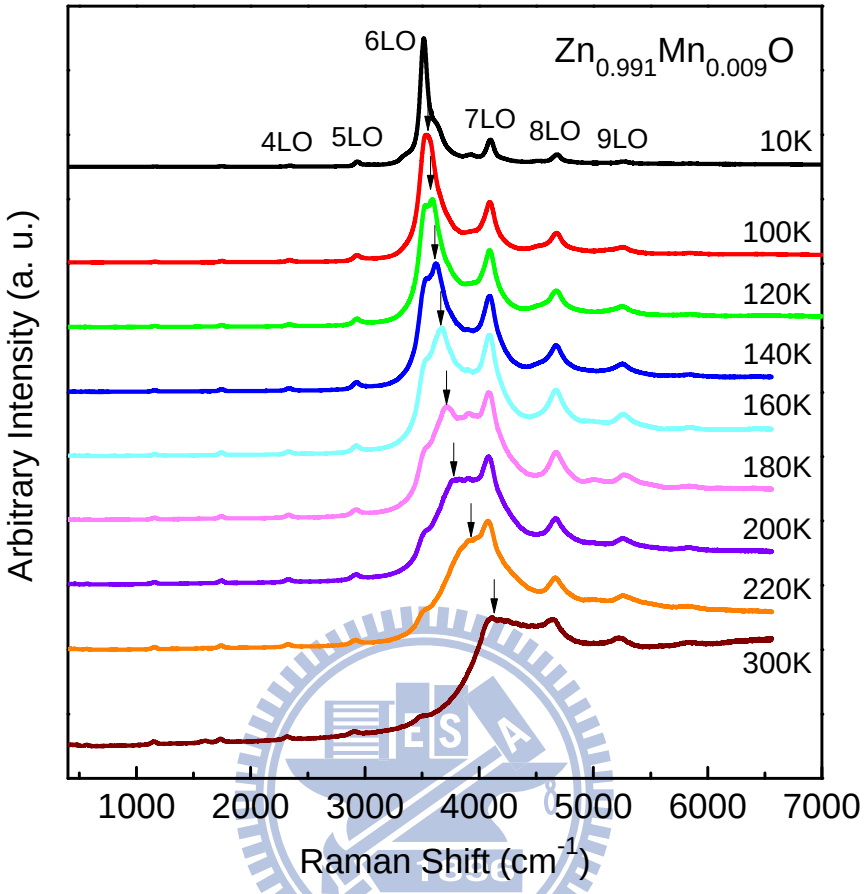

Fig. 3.10(a): Resonant Raman scatterings (RRS) of $Zn_{0.991}Mn_{0.009}O$ thin films with variable temperature, using the He-Cd laser (λ = 325 nm). The arrows show the PL positions.

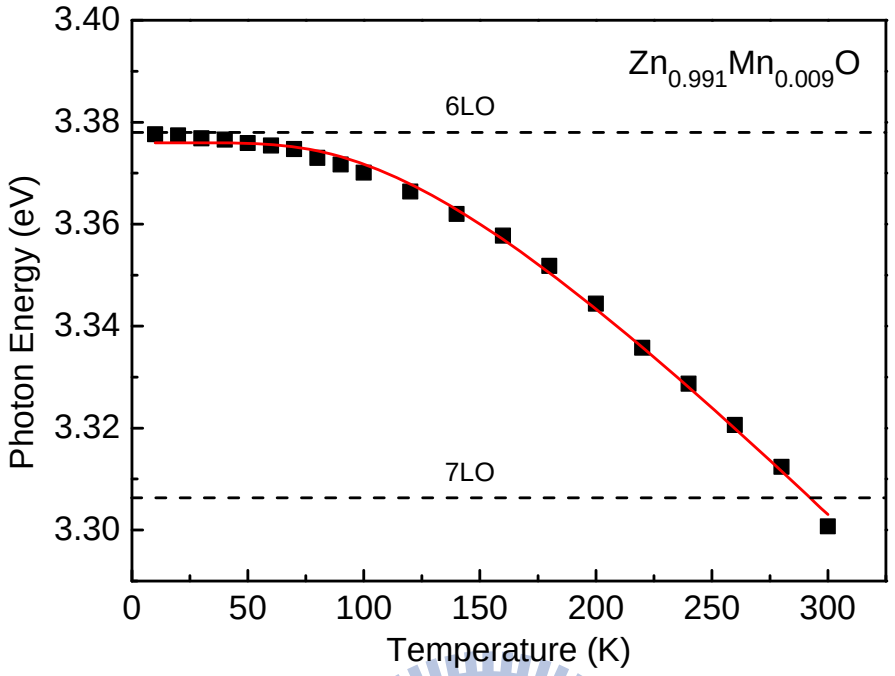

Fig. 3.10(b): Temperature dependent photoluminescence (PL) position of $Zn_{0.991}Mn_{0.009}O$. The solid curve describes the fit of these data by using the Bose-Einstein statistical factor for phonons. The dashed lines represents the energy positions of the scattered photons with energy $\hbar\omega \cong \hbar\omega_i - n\hbar\omega_{LO}$, $n = 6$ or 7.

3.2.4 Magneto-optical measurements

Fig. 3.11(a) and (b) show the low temperature (10 K) PL spectra of $Zn_{0.997}Mn_{0.003}O$ analyzed by ($\sigma+$) and ($\sigma-$) circular polarization at magnetic field B = 0 and B = 0.3 Tesla, respectively. At B = 0, no difference was observed between two circular polarization. The D^0X (at 3.363 eV) and RRS (at 3.306 eV and 3.378 eV) intensities for ($\sigma+$) and ($\sigma-$) components are approximately the same. However, at B = 0.3 Tesla, a slight difference is observed between the two circular polarization components of the D^0X. While the intensities of the two circular polarization components of the RRS remain the same. The degree of circular polarization can be defined as

$$P = \frac{I_{\sigma+} - I_{\sigma-}}{I_{\sigma+} + I_{\sigma-}}, \qquad (4)$$

where $I_{\sigma+}$ and $I_{\sigma-}$ are the intensities of the right and left circular polarization, respectively. For RRS, P = 0 at B = 0 and 0.3 Tesla. Whereas, for D^0X emission, P = 0 at 0 Tesla and P = 1.4 % at 0.3 Tesla. The non-zero circular polarization is due to the energy splitting of the two spin components of the D^0X, (electron -1/2 and hole -3/2) and (electron +1/2 and hole +3/2). Although, the energy separation is too small to be resolved, due the energy relaxation from the higher energy spin state to

the lower energy spin state, P = 1.4 % is observed. No hysteresis is observed. It implies that the $Zn_{0.997}Mn_{0.003}O$ exhibits para-magnetism due sp-d exchange between conduction band s electrons/valence band p holes and d electrons of the Mn atoms.

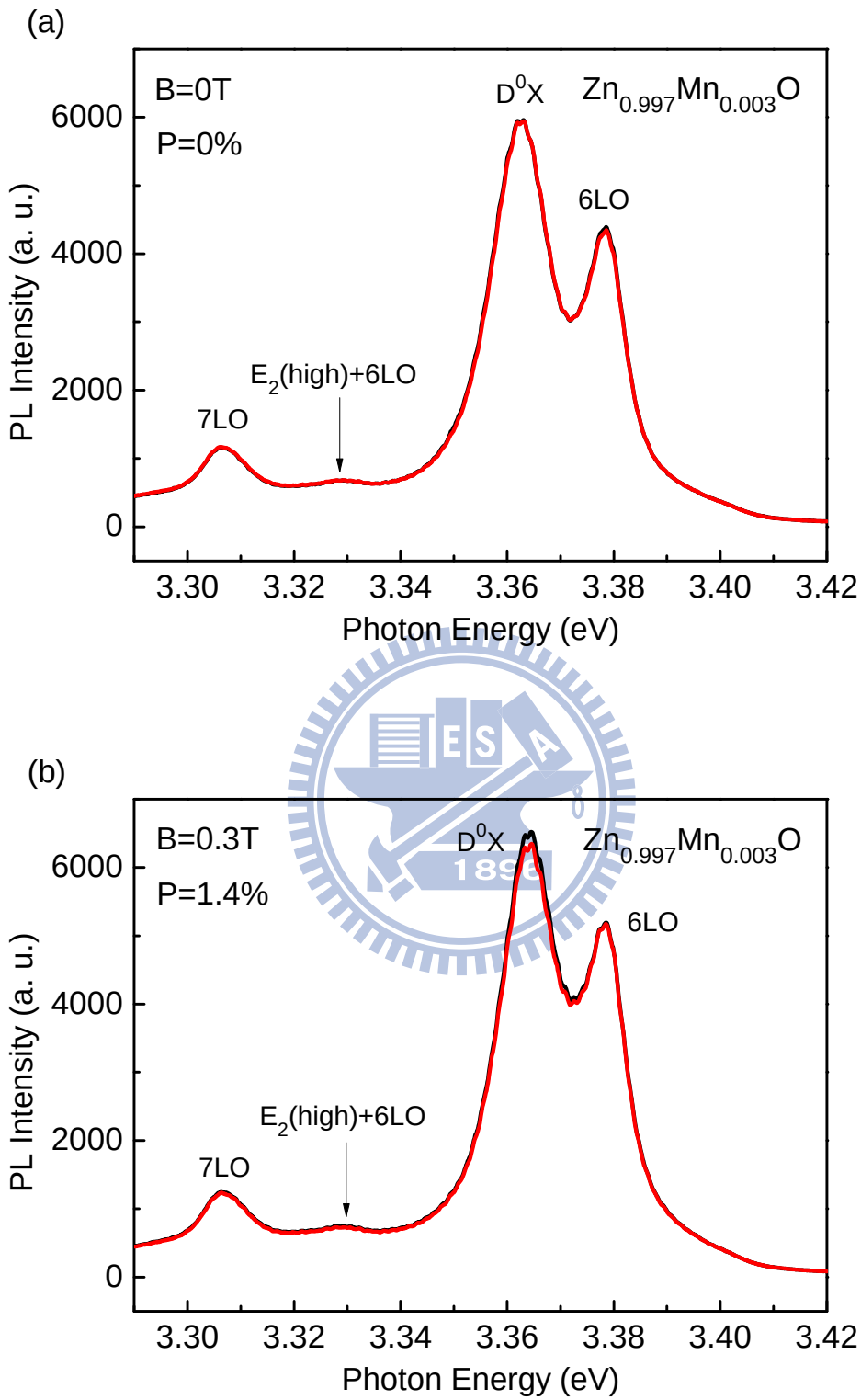

Fig. 3.11: Low temperature (10 K) PL spectra of $Zn_{0.997}Mn_{0.003}O$ (a) for B = 0 and (b) for B = 0.3 Tesla, respectively.

Chapter 4 Conclusion

We have grown ZnO and $Zn_{1-x}Mn_xO$ (x = 0.003 ~ 0.030) thin films by molecular beam epitaxy (MBE) system. X-ray diffraction (XRD) measurement reveals that these samples are all well aligned with the *c*-axis, and there are no second phases related to the Mn substitution. Transmittance measurement shows an increase of the band gap with the increasing Mn concentration. From RRS spectra, we observe LO phonon lines up to 5 and 11 order for ZnO and ZnMnO samples, respectively. From the temperature dependent RRS experiment, we find the intensities of these LO phonon lines are sensitive to the band gap position. Low temperature PL spectra of $Zn_{0.997}Mn_{0.003}O$ at magnetic field B = 0 T and 0.3 T were investigated to calculate the degrees of circular polarization of P = 0 % and 1.4 %, respectively.

Reference:

[1] J. K. Furdyna, *J. Appl. Phys.* **64**, R29 (1988).

[2] Y. Chen, D. M. Bagnall, H.J. Koh, K.T. Park, K. Hiraga, Z. Zhu, and T. Yao, *J. Appl. Phys.* **84**, 3912 (1998).

[3] T. Dietl, H. Ohno, F. Matsukara, J. Gilbert, and D. Ferrand, *Science* **287**, 1019 (2000).

[4] J. F. Scott, *Phys. Rev. B* **2**, 1209 (1970).

[5] H. M. Cheng, K. F. Lin, H. C. Hsu, C. J. Lin, L. J. Lin, and W. F. Hsieh, *J. Phys. Chem. B* **109**, 18385 (2005).

[6] M. F. Cerqueira, M. I. Vasilevskiy, F. Oliveira, A. G. Rolo, T. Viseu, J. Ayres de Campos, E. Alves, and R. Correia, *J. Phys. Condens. Matter* **23**, 334205 (2011).

[7] T. L. Phan, R. Vincent, D. Cherns, N. X. Nghia, and V. V. Ursaki, *Nanotechnology* **19**, 475702 (2008).

[8] R. Cusco, E. Alarcon-Llado, J. Ibanez, L. Artus, J. Jimenez, B. Wang, and M. J. Callahan, *Phys. Rev. B* **75**, 165202 (2007).

[9] E. Przezdziecka, E. Kaminska, M. Kiecana, M. Sawicki, L. Klopotowski, W. Pacuski, and J. Kossut, *Solid State Commun.* **139**, 541 (2006).

[10] M. Godlewski, A. Wasiakowski, V.Yu. Ivanov, A. Wojcik-Glodowska, M. Lukasiewicz, E. Guziewicz, R. Jakiela, K. Kopalko, A. Zakrzewski, and Y. Dumont, *Optical Materials* **32**, 680 (2010).

[11] Z. Yang, Z. Zuo, H. M. Zhou, W. P. Beyermann, and J. L. Liu, *J. Cryst. Growth* **314**, 97 (2011).

[12] J. S. Wang, C. S. Yang, M. J. Liou, C. X. Wu, K. C. Chiu, and W. C. Chou, *J. Crystal Growth* **310**, 4503 (2008).

[13] H. J. Ko, T. Yao, Y. Chen, and S. K. Hong, *J. Appl. Phys.* **92**, 4354 (2002).

[14] X. L. Wu, G. G. Siu, C. L. Fu, H. C. Ong, *Appl. Phys. Lett.* **78**, 2285 (2001).

[15] D. Y. Lin, H. J. Lin, J. S. Wu, W. C. Chou, C. S. Yang, and J. S. Wang, *J. Appl. Phys.* **105**, 053506 (2009).

[16] C. A. Johnson, K. R. Kittilstved, T. C. Kaspar, T. C. Droubay, S. A. Chambers, G. M. Salley, and D. R. Gamelin, *Phys. Rev. B* **82**, 115202 (2010).

[17] T. Mizokawa, T. Nambu, A. Fujimori, T. Fukumura, and M. Kawasaki, *Phys. Rev. B* **65**, 085209 (2002).

[18] K. W. Boer, *Survey of Semiconductor Physics: Electrons and Other*

Particles in Bulk Semiconductors; Van Nostrand Reinhold: New York, 1990; Chapter 28.

[19] J. F. Scott, T. C. Damen, W. T. Silfvast, R. C. C. Leite, and L. E. Cheesman, *Optics Commun.* **1**, 397 (1970).

[20] M. C. Klein, F. Hache, D. Ricard, and C. Flytzanis, *Phys. Rev. B* **42**, 11123 (1990).

[21] P. Lautenschlager, M. Garriga, and M. Cardona, *Phys. Rev. B* **36**, 4813 (1987).

[22] R. M. Martin and C. M. Varma, *Phys. Rev. Lett.* **26**, 1241 (1971).

[23] W. H. Sun, S. J. Chua, L. S. Wang, and X. H. Zhang, *J. Appl. Phys.* **91**, 4917 (2002).